International Journal of Thermophysics, Vol. 25, No. 5, September 2004 (© 2004)

Thermophysical Properties of Undercooled Liquid Cu–Ni Alloys[1]

G. Lohöfer,[2,3] J. Brillo,[2] and I. Egry[2]

Experimental data for the surface tension, density, and electrical resistivity of undercooled liquid Cu–Ni alloys of different compositions and at different temperatures are presented. The experiments were performed in facilities that combine the containerless positioning method of electromagnetic levitation with contactless measurement techniques. Although Cu–Ni alloys are rather simple from a chemical point of view, the data for density, surface tension, and electrical resistivity unveil the occurrence of short-range atomic order processes in the melt. For the density this manifests in a composition-dependent excess volume, for the surface tension in smaller values due to an increased surface segregation, and for the electrical resistivity in a deviation from the linear temperature dependence at low temperatures.

KEY WORDS: containerless processing; density; electrical resistivity; liquid Cu–Ni alloys; short-range atomic ordering; surface tension.

1. INTRODUCTION

Thermophysical properties of molten metals such as density, electrical resistivity, surface tension, and others play an important role in understanding the thermodynamic state of the liquid. Here we investigate copper–nickel alloys. First, they are of practical interest. Solid $Cu_{44}Ni_{56}$, known as constantan in electrical engineering, shows a constant electrical resistivity over a wide temperature range. Second, we are interested to find out, whether, despite the very low mixing enthalpy, there are cooperative effects in the melt between the copper and nickel atoms. And finally,

[1]Paper presented at the Fifteenth Symposium on Thermophysical Properties, June 22–27, 2003, Boulder, Colorado, U.S.A.

[2]Institute of Space Simulation, German Aerospace Center, D-51170 Köln, Germany.
[3]To whom correspondence should be addressed. E-mail: Georg.Lohoefer@dlr.de

0195-928X/04/0900-1535/0

the melt can easily be processed in our electromagnetic levitation facilities which leads to a reduction of the measurement errors.

From a chemical point of view the Cu–Ni alloys are rather simple. Copper and nickel are two metals with very similar properties concerning the density and the molar volume. Furthermore, in the liquid state, copper and nickel are totally miscible in all stoichiometric ratios and at all attainable temperatures [1]. Despite this similarity, our measurement data for density, surface tension, and electrical resistivity of these alloys in the liquid state show a clear deviation from an 'ideal' mixing behavior. This means, that the density, surface tension, and electrical resistivity of the mixture can not simply be derived without consideration of interactions between the constituents.

Cu–Ni alloys have a small, positive molar mixing enthalpy ΔH in the liquid state [2]. It can be described by

$$\Delta H = W_{\mathrm{Cu,Ni}} c_{\mathrm{Cu}} c_{\mathrm{Ni}} \quad \text{with} \quad W_{\mathrm{Cu,Ni}} \approx 11.5\,\mathrm{kJ \cdot mol^{-1}},$$

where c_{Cu} and c_{Ni} are the copper and nickel concentrations in the melt. This implies a maximum demixing temperature of ca. 425°C occurring for $Cu_{50}Ni_{50}$. Thus, we were interested to measure the above mentioned thermophysical quantities of the liquid Cu–Ni alloys also at very low temperatures in the undercooled state, i.e., in the liquid state below the melting temperature T_{m}, in order to investigate whether the occurrence of local atomic ordering processes in the melt already influence the global thermophysical properties.

To reduce disturbing influences of crucible walls on the measurements and to reach the deeply undercooled state of the Cu–Ni alloys, where possible ordering phenomena should be more pronounced, all measurements were performed contactlessly with containerlessly levitated melts. For containerless processing (positioning, heating and melting) of our Cu–Ni melt, we always used electromagnetic levitation [3]. For the contactless measurements, optical and inductive techniques were applied.

In the following sections we show data for the density, surface tension, and electrical resistivity of liquid Cu–Ni alloys at different temperatures and compositions and give a short overview of the applied measurement techniques.

2. DENSITY

In the past density measurements of liquid metals have been carried out on the copper–nickel system using electromagnetic levitation [4], the so-called maximum bubble pressure technique [5], and electrostatic levitation

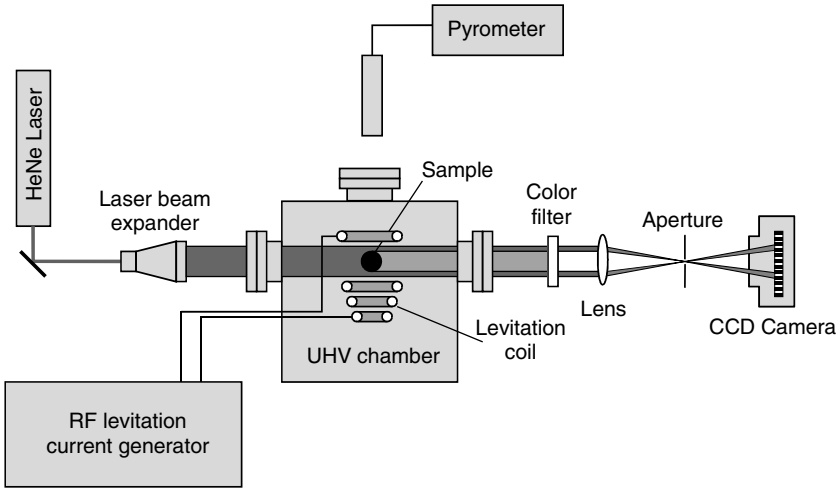

Fig. 1. Experimental setup for the density measurements. The shadow of the liquid, levitated sample inside the levitation coil, illuminated from the back by an expanded HeNe laser beam, is recorded by a CCD camera.

[6]. However, major differences in these results are common and, therefore, no reliable data are available until now. For our density measurements we used a new optical measurement technique combined with electromagnetic levitation.

2.1. Experimental Setup

The density was measured using the arrangement shown in Fig. 1. The sample was levitated and melted under argon atmosphere. As soon as the electromagnetic forces lift up the sample, currents that are induced inside the sample start heating it. Temperature control was maintained by carefully cooling the sample in a flow of argon gas. The temperature was measured using an infrared pyrometer. For measuring the density, i.e., the volume of the sample, it is of particular importance that the sample is fully visible from the side. We therefore designed a coil which assured that no part of the edge of the sample was hidden by the windings.

To measure the sample volume, an expanded, parallel HeNe laser beam was used to illuminate the sample from behind; see Fig. 1. The laser light is then focussed on the small aperture of a pinhole, which removes all nonparallel parts of the beam coming from interferences or the hot sample itself. Furthermore, a band-pass filter additionally blocks all light not originating from the laser. The shadow image of the sample is then captured

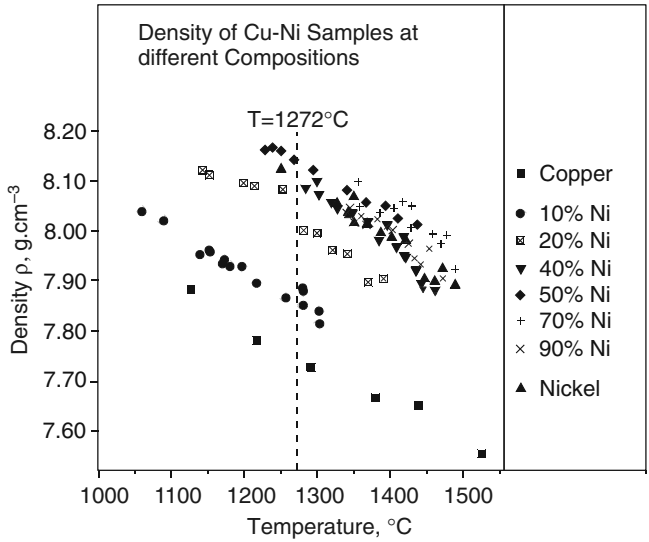

Fig. 2. Density data of liquid Cu–Ni alloys measured for different atomic fractions of Ni.

by means of a digital CCD camera, and fed into a computer. Finally, it is analyzed in real time by an edge detection algorithm. A calibration of the whole optical setup is performed by using very well defined ball-bearing spheres. This optical setup has the advantage to prevent apparent size changes due to sample movements along the optical axes, and to guarantee an always constant contrast for the shadow edge detection algorithm independent of the brightness of the hot sample.

2.2. Results and Discussion

Experimental data for the density $\rho(T)$ of different liquid Cu–Ni alloys are depicted in Fig. 2. It can be seen that the density data fit very well to a linear function of the temperature;

$$\rho(T) = \rho_{\mathrm{L}} + \rho_{\mathrm{T}}(T - T_{\mathrm{L}}). \tag{1}$$

In this equation, ρ_{L} is the density at liquidus temperature T_{L} and ρ_{T} is the thermal expansion coefficient. Their values for the different copper and nickel concentrations are listed in Table I. From these parameters, the density at all temperatures can be extrapolated. For a study of the concentration dependence of the density of liquid Cu–Ni, we use the values

Table I. Density Parameters ρ_L, ρ_T of Eq. (1) Together with the Liquidus Temperature T_L for Different Concentrations of the Liquid Cu–Ni Alloy, Taken from a Linear Fit to the Data Presented in Fig. 2

	T_L(°C)	ρ_L(g·cm^{-3})	ρ_T(10^{-4} g·cm^{-3}·°C^{-1})
Copper	1084	7.90	−7.65
$Cu_{90}Ni_{10}$	1136	7.97	−7.95
$Cu_{80}Ni_{20}$	1190	8.09	−9.57
$Cu_{60}Ni_{40}$	1280	8.13	−10.3
$Cu_{50}Ni_{50}$	1320	8.10	−7.72
$Cu_{30}Ni_{70}$	1380	8.06	−9.11
$Cu_{10}Ni_{90}$	1433	7.96	−9.26
Nickel	1454	7.92	−10.1

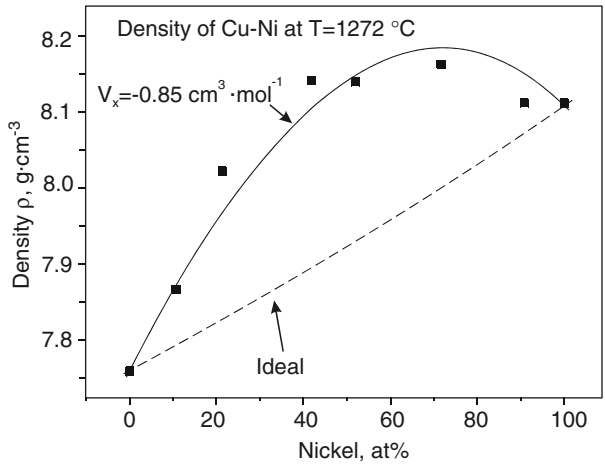

Fig. 3. Concentration dependence of the density of the liquid Cu–Ni alloys at 1272 °C. The dots represent the measurement values, the dashed line represents the behavior of the ideal solution model, and the solid line that of the regular solution model of Eq. (4).

calculated from Eq. (1) for $T = 1272°C$. Figure 3 shows a plot of these data.

For an 'ideal binary mixture', which assumes no interactions between components A and B of molar masses M_A and M_B and molar volumes V_A and V_B, the density $\rho(T)$ can be calculated at a specific temperature T according to the atomic fractions c_A and $c_B = 1 - c_A$ with

$$\rho(T) = \frac{c_A M_A + c_B M_B}{c_A V_A(T) + c_B V_B(T)} = \frac{c_A M_A + c_B M_B}{c_A \frac{M_A}{\rho_A(T)} + c_B \frac{M_B}{\rho_B(T)}}, \tag{2}$$

where ρ_A, ρ_B are the densities of pure substances A and B at temperature T. For the densities and molar masses of liquid copper and nickel at 1272 °C the behavior of Eq. (2) is represented by the dashed line in Fig. 3, showing that a Cu–Ni alloy is not composed of independent components. Instead, the total volume must be corrected by the 'excess volume' V_E, which accounts for an interaction between the alloy components. For this we choose the simple symmetric approach,

$$V_E = c_A c_B V_X \tag{3}$$

with V_X being a constant parameter, independent of temperature and concentration. The density for a binary mixture can then be written as

$$\rho = \frac{c_A M_A + c_B M_B}{c_A \frac{M_A}{\rho_A} + c_B \frac{M_B}{\rho_B} + c_A c_B V_X}. \tag{4}$$

For the densities and molar masses of liquid copper and nickel at 1272 °C the fit of Eq. (4) to the measured density data now yields $V_X = -0.85\,\mathrm{cm^3 \cdot mol^{-1}}$, which is in much better agreement. The corresponding graph is represented by the solid line in Fig. 3. Note, that the excess volume V_E is negative, implying that the total volume of the mixture is smaller than the sum of the single Cu and Ni melt volumes.

We assume that this result follows mainly from pure geometrical arrangements of the copper and nickel atoms in the liquid. An influence of the mixing enthalpy can probably be excluded, because the temperature of 1272 °C is far away from the maximum demixing temperature of ca. 425 °C, and because the demixing tendency of this alloy should, on the contrary, even enlarge the excess volume. More details of the results and the experimental setup for the density measurement can be found in Refs. 7 and 8.

3. SURFACE TENSION

3.1. Experimental Setup

The experimental setup for the surface tension measurements, see Fig. 4, is similar to that for the density measurements. The Cu–Ni sample is levitated and melted within a quartz-glass tube filled with a mixture of helium and hydrogen, whereas the magnetic levitation coils are located outside the glass tube. The temperature is measured by a pyrometer and

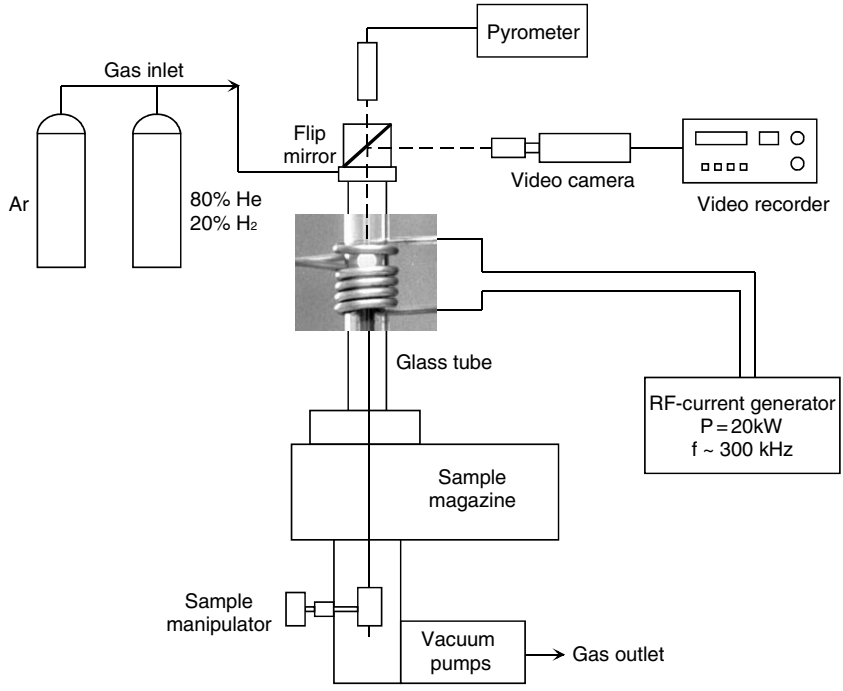

Fig. 4. Experimental setup for the surface tension measurements. The sample is levitated in a quartz tube. The temperature and surface oscillations of the droplet are alternatively observed from the top over a mirror by a pyrometer or a video camera.

controlled by the gas flow. The turbulent fluid flow of the Cu–Ni melt, excited by the strong rf magnetic levitation field, causes oscillations of the droplet surface which is recorded by a camera. As a containerless technique, electromagnetic levitation has the advantage that the oscillations of the liquid droplet can be observed without distortions from mechanical contact with a support.

From the camera image the 'oscillating drop method' evaluates, by Fourier analysis, the surface oscillation frequencies of the sample around its equilibrium shape. For a nonrotating, spherical sample the relation between the oscillation frequency ω_R of the least damped oscillation mode and the surface tension γ is given by the Raleigh law

$$\omega_R^2 = \frac{32\pi}{3}\frac{\gamma}{M}, \tag{5}$$

where the mass M of the droplet is determined by weighing. For rotating, nonspherical droplets, which generally occur in ground-based levitation

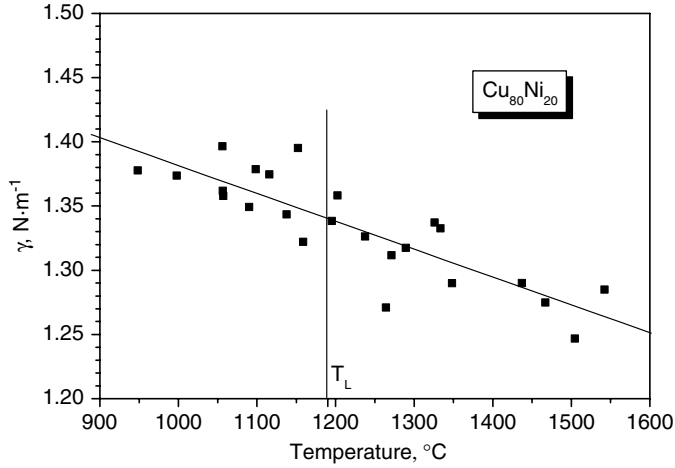

Fig. 5. Surface tension data of liquid $Cu_{80}Ni_{20}$.

facilities, corrections have to be applied. More details of this measurement method can be found, e.g., in Ref. 9.

3.2. Results and Discussion

Representative of other concentrations, Fig. 5 shows the temperature-dependent experimental data for the surface tension $\gamma(T)$ of the liquid $Cu_{80}Ni_{20}$ alloy. The behavior of $\gamma(T)$ is sufficiently well described by a linear temperature dependence,

$$\gamma(T) = \gamma_L + \gamma_T(T - T_L), \tag{6}$$

where γ_L is the surface tension at the liquidus temperature T_L, and γ_T is the thermal coefficient. Their values for the different copper and nickel concentrations are listed in Table II.

For an investigation of interactions between the copper and nickel atoms in the melt the representation of the dependence of γ on the concentration, as shown in Fig. 6 for 1277 °C, is more interesting. To understand the behavior of γ, we note that for each alloy component i the surface tension can be defined as the difference between the chemical potential at the surface μ^S and in the bulk μ^B divided by the number of atoms per surface area a [10];

$$\gamma = \frac{\mu_i^S - \mu_i^B}{a_i} = \frac{\mu_{i,\text{pure}}^S + \mu_{i,\text{mix}}^S - (\mu_{i,\text{pure}}^B + \mu_{i,\text{mix}}^B)}{a_i} = \gamma_i + \frac{\mu_{i,\text{mix}}^S - \mu_{i,\text{mix}}^B}{a_i}. \tag{7}$$

Table II. Surface Tension Parameters γ_L, γ_T of Eq. (6) Together with the Liquidus Temperature T_L for Different Concentrations of the Liquid Cu–Ni Alloy, Taken from a Linear Fit to the Experimental Data

	T_L(°C)	γ_L(N·m^{-1})	γ_T(10^{-4} N·m^{-1}·°C^{-1})
Copper	1084	1.30	−2.34
$Cu_{90}Ni_{10}$	1136	1.31	−2.21
$Cu_{80}Ni_{20}$	1190	1.34	−2.17
$Cu_{70}Ni_{30}$	1235	1.32	−3.24
$Cu_{60}Ni_{40}$	1280	1.36	−1.91
$Cu_{50}Ni_{50}$	1320	1.37	−0.94
$Cu_{40}Ni_{60}$	1347	1.38	−0.45
$Cu_{30}Ni_{70}$	1380	1.43	−0.84
$Cu_{20}Ni_{80}$	1417	1.51	−0.21
$Cu_{10}Ni_{90}$	1433	1.61	−0.67
Nickel	1454	1.77	−3.30

For an ideal solution of the two alloy components, where no interactions take place, we know from thermodynamics that

$$\mu_{i,\mathrm{mix}}^{\mathrm{S,B}} = RT \log(c_i^{\mathrm{S,B}}), \tag{8}$$

so that in our case,

$$\gamma = \gamma_{\mathrm{Cu}} + \frac{RT}{a_{\mathrm{Cu}}} \log\left(\frac{c_{\mathrm{Cu}}^{\mathrm{S}}}{c_{\mathrm{Cu}}^{\mathrm{B}}}\right) = \gamma_{\mathrm{Ni}} + \frac{RT}{a_{\mathrm{Ni}}} \log\left(\frac{1-c_{\mathrm{Cu}}^{\mathrm{S}}}{1-c_{\mathrm{Cu}}^{\mathrm{B}}}\right). \tag{9}$$

First of all, it is obvious that differences in the surface tension between the alloy γ and its single components γ_i result in a surface segregation, i.e., in different concentrations of the components at the surface c_i^{S} and in the bulk c_i^{B}. Furthermore, it is evident that the dashed line in Fig. 6, resulting from Eq. (9), where the surface concentration $c_{\mathrm{Cu}}^{\mathrm{S}}$ has been eliminated by the second equality in Eq. (9), does not fit the data points very well. A more detailed analysis, which also considers the demixing and ordering tendency of the Cu–Ni alloy, quantitatively described by the mixing enthalpy $\Delta H = W_{\mathrm{Cu,Ni}} c_{\mathrm{Cu}} c_{\mathrm{Ni}}$, and leading to an increased surface segregation, satisfies the observations much better. More details about the surface tension measurements of the Cu–Ni alloys can be found in Refs. 10 and 11.

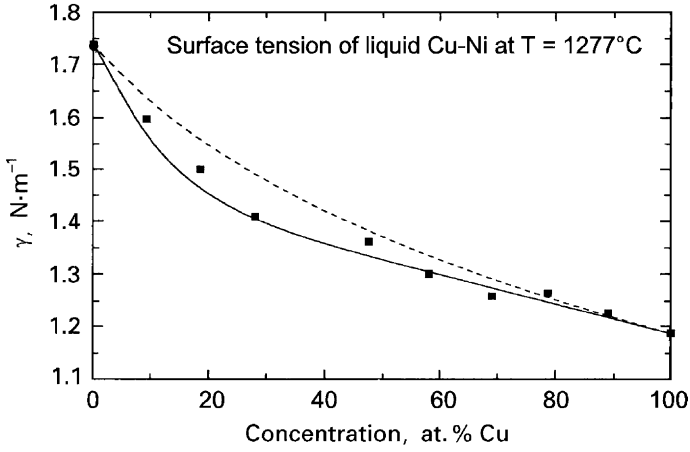

Fig. 6. Concentration dependence of the surface tension of the liquid Cu–Ni alloys at 1277 °C. The dots represent the measurement values, the dashed line represents the behavior of the ideal solution model, and the solid line that of the regular solution model.

4. ELECTRICAL RESISTIVITY

Noncontact electrical resistivity measurements on liquid metal samples can be performed by use of electromagnetic induction [12,13]. However, conventional methods generally employ crucibles for the containment of the melt. We have instead combined this measurement technique with the electromagnetic levitation method by placing a levitation coil around a pair of measurement coils to keep the sample completely untouched.

4.1. Experimental Setup

Figure 7 shows the arrangement of our measuring transformer between the levitation coils. The alternating current I_1 in the primary coil of the transformer generates a high frequency magnetic field that induces a voltage U_2 in the secondary coil, which depends on the electrical resistivity r of the sample, its radius R, and the deviation of its shape from spherical symmetry α;

$$\left|\frac{U_2}{I_1}\right| e^{i\varphi} = Z(r, R, \alpha) \tag{10}$$

By measurement of the absolute values of I_1 and U_2 as well as the phase difference φ between both, the (complex) impedance $Z(r, R, \alpha)$ is determined. In the next step the electrical resistivity of the liquid droplet is

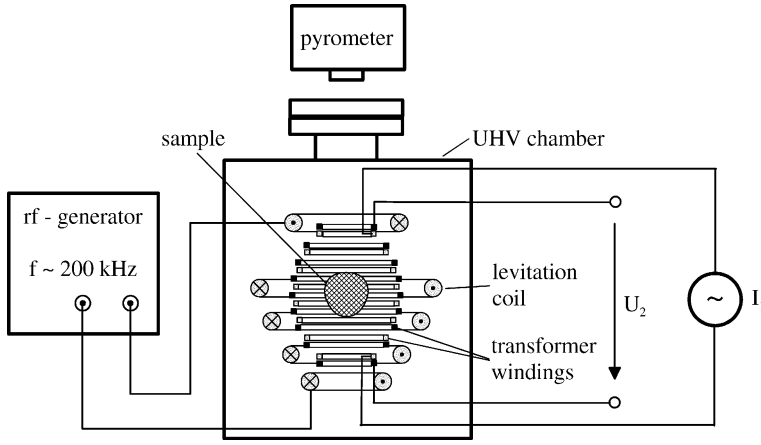

Fig. 7. Experimental setup for the electrical resistivity measurements. The primary (gray squares) and secondary (black squares) measurement coils are integrated with the surrounding levitation coil in an UHV chamber.

calculated from the theoretical relation between Z and r, which is well known except for calibration constants that depend on the radius R and the shape factor α. In order to determine these constants, all measurements are performed at different current frequencies in the range between 10 kHz and 1 MHz. Furthermore, a calibration experiment with a spherical sample of well defined resistivity and radius has to be carried out.

During the measurement the sample is containerlessly positioned by the levitation field in the center of the measurement transformer. To prevent inductive interactions between the high frequency magnetic levitation field and the measuring coils, the measurement itself is performed only in short-time intervals of about 1 ms duration, during which the levitation field is completely switched off. More details of the experiment facility can be found in Ref. 14 and especially in Ref. 15.

4.2. Results and Discussion

Experimental data for the electrical resistivity $r(T)$ of different liquid Cu–Ni alloys are presented in Fig. 8. It can be seen that weak deviations from the typical linear temperature behavior occur for nickel fractions $c_{\mathrm{Ni}} = 0.2$ and $c_{\mathrm{Ni}} = 0.4$, which we describe for simplicity by a polynomial temperature function,

$$r(T) = r_0 + r_{T1}T + r_{T2}T^2. \tag{11}$$

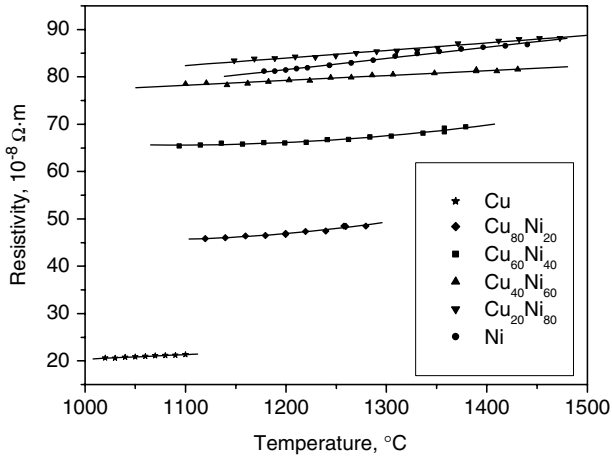

Fig. 8. Resistivity data of liquid Cu–Ni alloys measured for different atomic fractions. For nickel fractions of 20 and 40% there are weak deviations from the typical linear temperature behavior.

Table III. Resistivity Parameters r_L, r_{T1}, and r_{T2} of Eq. (11) for Different Concentrations of the Liquid Cu–Ni Alloy, Taken from a Fit to the Data Presented in Fig. 8

	$r_0(10^{-8}\Omega\cdot\mathrm{m})$	$r_{T1}(10^{-10}\,\Omega\cdot\mathrm{m}\cdot{}^\circ\mathrm{C}^{-1})$	$r_{T2}(10^{-13}\,\Omega\cdot\mathrm{m}\cdot{}^\circ\mathrm{C}^{-2})$
Copper	10.9	0.945	0.0
$Cu_{80}Ni_{20}$	113	−12.9	6.11
$Cu_{60}Ni_{40}$	118	−9.61	4.40
$Cu_{40}Ni_{60}$	66.8	1.04	0.0
$Cu_{20}Ni_{80}$	64.9	1.59	0.0
Nickel	52.3	2.40	0.0

The coefficients r_0, r_{T1}, and r_{T2}, which are listed for different concentrations in Table III, result from fits to the measured data. To understand the behavior of $r(T)$ we note that the electrical resistivity in nonordered liquid metals is caused by the scattering of the free valence electrons by the electric potential of the remaining ions of charge Ze [16]. Essentially three effects have an influence on the scattering and thus on the resistivity.

(1) The basic part in the resistivity results from the scattering of the electrons at the randomly distributed Cu and Ni ions of uniform density and concentration. This is expressed mainly by the constant term r_0 in Eq. (11). Due to the differences in atomic radii

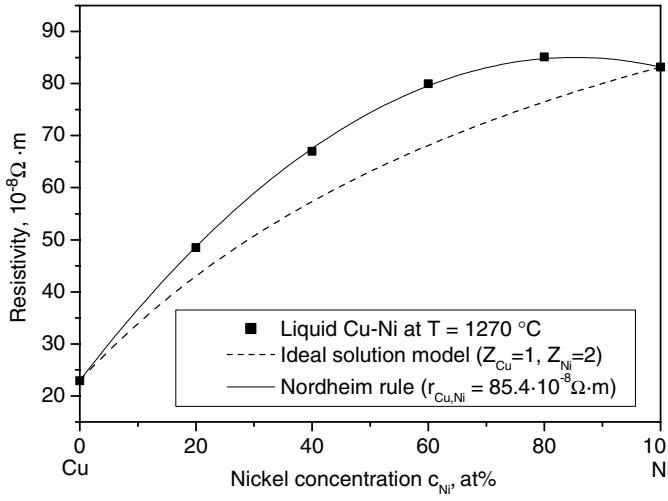

Fig. 9. Concentration dependence of the electrical resistivity of the liquid Cu–Ni alloys at 1270 °C. The dashed line represents the ideal solution model. The solid line is a fit of the Nordheim rule to the data points.

or densities of the two components, which have an influence on the scattering cross section, this term still depends on the Cu–Ni concentrations.

(2) For increasing temperature, density fluctuations of the ions proportional to the thermal energy kT occur, which locally change the scattering potential and thus the electrical resistivity. This is expressed mainly by the second term in Eq. (11).

(3) Other contributions to $r(T)$ result from differences in the valence numbers of the Cu and Ni ions, i.e., from $Z_{Cu} \neq Z_{Ni}$. In this case the scattering potential changes also by a variation of the Cu–Ni concentration. This can be caused by

   (a) a uniform concentration change resulting in the concentration dependence of the resistivity as shown in Fig. 9;

   (b) local concentration fluctuations (structural ordering of the ions), which increase with decreasing temperature due to the positive mixing enthalpy of the Cu–Ni alloys. The resulting changes in the local scattering potential give rise to the observed deviation from the linear temperature dependence.

Without interactions between the copper and nickel components in the alloy, expressed by the positive mixing enthalpy, and the resulting structural ordering of the ions, the observed deviation from the typical linear temperature behavior of the resistivity cannot be explained. Details of these results can also be found in Ref. 17.

But also the concentration dependence of the electrical resistivity for a fixed temperature, shown in Fig. 9, indicates nonideal solution behavior of the liquid Cu–Ni alloys. Assuming Drude's free electron gas model for the valence electrons scattered by randomly distributed metal ions, the resistivity can be expressed by

$$r = \frac{m_e}{n_e e^2} \frac{1}{\tau}, \tag{12}$$

where m_e, n_e, and e are the electron mass, particle density, and charge, respectively, and where τ, interpreted as the mean total collision time, depends on the interaction between the electrons and ions. If the collision of an electron with an ion is not influenced by any neighboring ion, which also implies that there are no interactions between the different types of ions (ideal solution), then the total number of electron–ion collisions per unit time is just the sum of the collisions with the single ion components, i.e., $1/\tau = \sum_i 1/\tau_i$, and we may use results from ideal gas theory (see e.g., Ref. 18, Chap. 5) $1/\tau_i \propto n_i Q_i$, where n_i and Q_i are the particle density and mean scattering cross section of ion component i, respectively. With the electron density given by $n_e = \sum_i n_i Z_i$, where Z_i is the valence electron number of component i, the resistivity now reads $r \propto \sum_i c_i Q_i / \sum_i c_i Z_i$ or with the known resistivities of the pure components $r_i := r(c_i = 1)$,

$$r = \frac{\sum_i c_i Z_i r_i}{\sum_i c_i Z_i}. \tag{13}$$

Taking for Z_i the number of the s-band electrons, the result of the ideal solution model for the electrical resistivity of the Cu–Ni alloys, where $Z_{Cu} = 1$ and $Z_{Ni} = 2$, is shown by the dashed line in Fig. 9. It reflects the right tendency, but cannot explain the maximum of the data points near $c_{Ni} \approx 0.8$ even for different values of Z_{Cu} and Z_{Ni}. The remaining discrepancy results mainly from the inherent assumption of individual electron-ion scatterings, which generally hold in rarefied plasmas but not in dense liquids. In the latter, not only does the field of a single ion take part in the scattering process but also that of its neighbors. Application of Eq. (13) to this case implicitly assumes Q_i to be an effective cross section resulting from the superposition of all scattering fields of the i-th component, which, as well as the valence number Z_i, also depend on quantum mechanical interactions between the ions.

Analyzing the experimental resistivity data for the liquid Cu–Ni alloy, shown in Fig. 9, we recognize that near $c_{\mathrm{Ni}} \approx 1$ the replacement of strongly scattering Ni-ions by more weakly scattering Cu-ions does not reduce the alloy resistivity, as expected from the ideal model of Eq. (13), but even increases it. The density increase, shown in Fig. 3, is too small to describe this effect sufficiently well. Consequently, in a dense liquid also the influence of the quantum mechanical interactions between different alloy components on the electron scattering has to be considered. We do this phenomenologically by introducing an additional cross section Q_{ij}. With this assumption, the above formula for the resistivity expands to

$$r = \frac{C \sum_i c_i \left(Q_i + \sum_{j \neq i} c_j Q_{i,j} \right)}{\sum_i c_i Z_i} = \frac{\sum_i c_i Z_i r_i \left(1 + \sum_{j \neq i} c_j Q_{i,j}/Q_i \right)}{\sum_i c_i Z_i}, \quad (14)$$

where on the right-hand side the constant of proportionality C has been replaced by the known resistivities of the pure components $r_i := r(c_i = 1)$. The remaining unknown, normalized quantity $Q_{i,j}/Q_i$ can be used as a fit parameter. For the two-component Cu–Ni alloy the assumption $Z_{\mathrm{Cu}} = Z_{\mathrm{Ni}}$ transforms Eq. (14) into the well known Nordheim rule,

$$r = c_{\mathrm{Ni}} r_{\mathrm{Ni}} + (1 - c_{\mathrm{Ni}}) r_{\mathrm{Cu}} + c_{\mathrm{Ni}} (1 - c_{\mathrm{Ni}}) r_{\mathrm{Ni,Cu}}, \quad (15)$$

which fits the data points extremely well with $r_{\mathrm{Ni,Cu}} = 85.4 \times 10^{-8}\ \Omega\cdot\mathrm{m}$, as shown by the solid line in Fig. 9.

5. SUMMARY

We presented experimental data for the density, surface tension, and electrical resistivity of undercooled liquid Cu–Ni alloys of different compositions and at different temperatures. All quantities show deviations from the typical behavior of an ideal solution implying that interactions between the copper and nickel atoms in the melt have to be taken into account. For the density this manifests itself by the negative excess volume, which means that the molar volume of the mixture is smaller than the sum of the molar volumes of the constituents. For the surface tension this is demonstrated by the measurement of smaller values than expected due to enhanced surface segregations. And finally, for the electrical resistivity, this results in a deviation from linear temperature dependence and in a maximum value near a concentration of $c_{\mathrm{Ni}} \approx 0.8$.

ACKNOWLEDGMENT

The support of this work by the "Deutsche Forschungsgemeinschaft" is gratefully acknowledged.

REFERENCES

1. T. B. Massalski, *Binary Alloy Phase Diagrams* (Americans Society of Metals, Materials Park, Ohio, 1986).
2. S. Srikanth and K.T. Jacob, *Mat. Sci. Technol*. **5**:427 (1989).
3. P. R. Sahm, I. Egry, and T. Volkmann, *Schmelze, Erstarrung, Grenzfläche* (Vieweg, Wiesbaden, 1999).
4. S. Y. Shiraishi and R. G. Ward, *Can. Met. Quat*. **3**:117 (1964).
5. A. Saito and S. Watanabe, *Nipp. Kinz. Gakk*. **35**:554 (1971).
6. S. K. Chung, D. B.Thiessen, and W. K. Rhim, *Rev. Sci. Instrum*. **67**:3175 (1996).
7. J. Brillo and I. Egry, *Z. Metallkd*. **95**:691 (2004).
8. J. Brillo and I. Egry, *Int. J. Thermophys*. **24**:1155 (2003).
9. S. Schneider, I. Egry, and I. Seyhan, *Int. J. Thermophys*. **23**:1241 (2002).
10. E. Gorges and I. Egry, *J. Mater. Sci*. **30**:2517 (1995).
11. E. Gorges, *Bestimmung der Dichte und Oberflächenspannung von levitierten flüssigen Metallegierungen am Beispiel des Systems Kupfer–Nickel* (Ph.D. Thesis, RWTH Aachen, Aachen, 1996).
12. Ya. A. Kraftmakher, *Meas. Sci. Technol*. **2**:253 (1991).
13. J. E. Enderby, S. Ansell, S. Krishnan, D. L. Price, and M.-L. Saboungi, *Appl. Phys. Lett*. **71**:116 (1997).
14. T. Richardsen and G. Lohöfer, *Int. J. Thermophys*. **20**:1029 (1999).
15. T. Richardsen, *Ein induktives Messverfahren zur Bestimmung der elektrischen Leitfähigkeit an unterkühlten Metallschmelzen* (Shaker, Aachen, 2001).
16. S. Takeuchi and H. Endo, *Trans. JIM* **3**:35 (1962).
17. T. Richardsen, G. Lohöfer, and I. Egry, *Int. J. Thermophys*. **23**:1207 (2002).
18. S. Chapman and T. G. Cowling, *The Mathematical Theory of Non-uniform Gases* (University Press, Cambridge, 1991).